

Topological Floquet edge states in periodically curved waveguides

Bo Zhu,^{1,2} Honghua Zhong,^{1,3} Yongguan Ke,^{1,2} Xizhou Qin,¹
 Andrey A. Sukhorukov,⁴ Yuri S. Kivshar,⁴ and Chaohong Lee^{1,2,5,*}

¹Laboratory of Quantum Engineering and Quantum Metrology, School of Physics and Astronomy,
 Sun Yat-Sen University (Zhuhai Campus), Zhuhai 519082, China

²State Key Laboratory of Optoelectronic Materials and Technologies,
 Sun Yat-Sen University (Guangzhou Campus), Guangzhou 510275, China

³Institute of Mathematics and Physics, Central South University of Forestry and Technology, Changsha 410004, China

⁴Nonlinear Physics Centre, Research School of Physics and Engineering,
 The Australian National University, Canberra ACT 2601, Australia

⁵Synergetic Innovation Center for Quantum Effects and Applications,
 Hunan Normal University, Changsha 410081, China

(Dated: December 14, 2024)

We study the Floquet edge states in arrays of periodically curved optical waveguides described by the modulated Su-Schrieffer-Heeger model. Beyond the bulk-edge correspondence, our study explores the interplay between band topology and periodic modulations. By analysing the quasi-energy spectra and Zak phase, we reveal that, although topological and non-topological edge states can exist for the same parameters, *they can not appear in the same spectral gap*. In the high-frequency limit, we find analytically all boundaries between the different phases and study the coexistence of topological and non-topological edge states. In contrast to unmodulated systems, the edge states appear due to either band topology or modulation-induced defects. This means that periodic modulations may not only tune the parametric regions with nontrivial topology, but may also support novel edge states.

Recently, topology has emerged as a new approach to manipulate properties of light under continuous deformations [1]. Electromagnetic topological states have been found in both microwave [2–4] and optical [5–7] regimes. Similar to topological insulators for electrons, photonic topological insulators have also been created [1–16]. Beyond conventional topological phenomena in linear Hermitian systems, topological gap solitons have been found in nonlinear optical systems [17], and it was shown that topological states can survive in non-Hermitian systems [18]. Moreover, periodic modulations can bring several novel topological properties usually absent in their non-modulated analogues [9, 19–26].

Bulk-edge correspondence [27, 28] is a well-established principle for two-dimensional (2D) topological systems. It establishes the exact correspondence between bulk states subjected to periodic boundary conditions (PBCs) and edge states in the systems with open boundary conditions (OBCs). Up to now, topological edge states have been found in several 2D photonic systems [10, 13, 29, 30]. However, for one-dimensional (1D) lattice models, edge states have been shown to appear in periodically modulated but non-topological lattices [31, 32]. This suggests that edge states can be induced by either topology or periodic modulations. Here, *we wonder whether topological and non-topological edge states may coexist* and, if they may coexist, how to distinguish between topological and non-topological edge states.

In this Letter, we study the Floquet edge states (FESs) in arrays of periodically curved optical waveguides described by a periodically modulated Su-Schrieffer-Heeger (SSH) model [33]. We analyse, for the first time to our

knowledge, the interplay between band topology and periodic modulations, and describe the coexistence of both topological and non-topological edge states supported by the same parameters. Our results show that, for a specific gap, the Zak phase Z_{G_m} is either 0 or π , so that the topological edge states appear only in the gap of $Z_{G_m} = \pi$. Through controlling both modulation frequency and amplitude, we may drive the system from non-topological to topological regime, and vice versa. We demonstrate analytically that periodic modulations induce *a virtual defect at the boundary*, being the key mechanism for the formation of non-topological edge states.

We consider a 2D array of coupled optical waveguides, where the waveguides are periodically curved along the longitudinal propagation direction, see Fig. 1. The light field $\psi(x, y, z)$ obeys the paraxial wave equation

$$-i\frac{\partial\psi}{\partial z} = \frac{\lambda'}{4\pi n'}\left(\frac{\partial^2}{\partial x^2} + \frac{\partial^2}{\partial y^2}\right)\psi + \frac{2\pi}{\lambda'}\nu(x, y, z)\psi, \quad (1)$$

where λ' is the optical wavelength in vacuum, n' is the medium refractive index, and $\nu(x, y, z)$ describes the refractive index variation at the waveguide positions. The waveguide centers $x_n(z) = x_n(z + T)$ are periodically curved along the longitudinal direction with the curving period T much larger than the inter-waveguide distance Δx . Here we set $x_n(z) = n\Delta x + A[\cos(\omega z) - 1]$ with the modulation amplitude A and the modulation frequency ω . By implementing the coordinate transformation: $[\hat{z} = z, \hat{y} = y, \hat{x}(z) = x - x_0(z)]$, we have $\partial_x = \partial_{\hat{x}}$, $\partial_y = \partial_{\hat{y}}$ and $\partial_z = \partial_{\hat{z}} - \dot{x}_0\partial_{\hat{x}}$. Then, after applying the gauge transformation and coupled-mode expansion, we

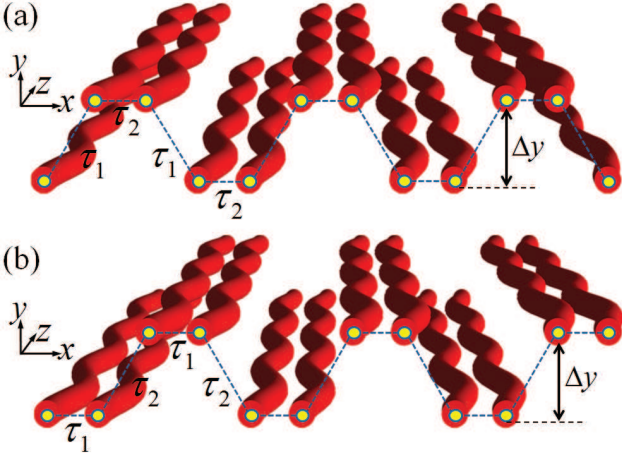


Figure 1. Schematic diagram of waveguide arrays curved along the propagation direction of light (z -axis). The center-to-center spacing along the x -axis is fixed as Δx , and the one along the y -axis is either 0 or Δy intermittently. The coupling strength is either τ_1 or τ_2 intermittently. (a) $\tau_1/\tau_2 < 1$ with $\tau_2 = \tau$, and (b) $\tau_1/\tau_2 > 1$ with $\tau_1 = \tau$.

derive the coupled-mode equations

$$-i \frac{du_n}{dz} = \tau_n \exp[i\eta A\omega(\hat{x}_{n+1} - \hat{x}_n) \sin(\omega z)] u_{n+1} + \tau_{n-1} \exp[-i\eta A\omega(\hat{x}_n - \hat{x}_{n-1}) \sin(\omega z)] u_{n-1}. \quad (2)$$

Here $\eta = 2\pi n'/\lambda'$, u_n denotes the complex field amplitude for the n -th waveguide with n being the waveguide index. As the center-to-center waveguide spacing along the x -axis is constant (i.e. $\hat{x}_{n+1} - \hat{x}_n = \hat{x}_n - \hat{x}_{n-1} = \Delta\hat{x}$) and one along the y -axis is either 0 or Δy intermittently, the hopping strengths can be written as $\tau_n = \frac{1}{2}\{[1 - (-1)^n]\tau_1 + [1 + (-1)^n]\tau_2\}$ and the maximum hopping strength $\tau = \max\{\tau_1, \tau_2\}$ is fixed. By adjusting the distance $\Delta\hat{y}$, one may tune the values of τ_n . Without loss of generality, we set $\eta = 1$ and $\tau = 1$.

Since the system is invariant under $z \rightarrow z + T$, according to the Floquet theorem [20] we have $u_n(z) = e^{-iEz} \sum_{\chi=-\infty}^{+\infty} e^{-i\chi\omega z} c_{n,\chi}$, where $c_{n,\chi}$ is the amplitude of the χ -th Floquet state. Substituting the above Floquet expansion into the coupled-mode equations, one obtains quasi-energy equation in the Floquet space. We introduce the average over one modulation period for all z -dependent quantities and obtain the quasi-energy eigenmode equation, $Ec_{n,\chi} = \sum_{\chi'=-\infty}^{+\infty} \tau_{n-1} J_{\chi-\chi'} c_{n-1,\chi'} + \sum_{\chi'=-\infty}^{+\infty} \tau_n J_{\chi'-\chi} c_{n+1,\chi'} + \chi\omega c_{n,\chi}$, where $J_{\chi'-\chi}$ is the Bessel function $J_{\chi'-\chi}(A\omega)$. To obtain the quasi-energy spectrum, one needs to truncate the Floquet space. In our calculation, we choose $\chi', \chi \in [-X, X]$ and $Y = 2X + 1$ is the truncation number.

Now we discuss the quasi-energy spectra under OBC.

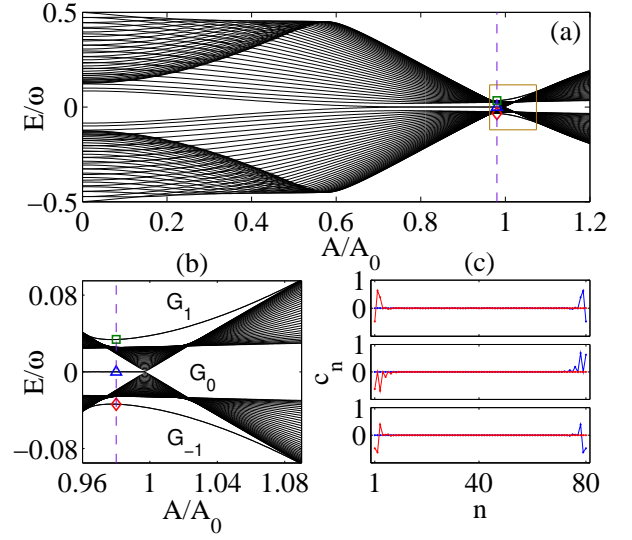


Figure 2. Quasi-energy spectra under open boundary condition. (a) Scaled quasi-energy E/ω vs. the scaled modulation amplitude A/A_0 . (b) Enlarged rectangular region of (a). (c) The Floquet edge states corresponding to the square, triangle, and diamond points in the three gaps (G_{+1}, G_0, G_{-1}) at $A/A_0 = 0.98$ marked in (b). The parameters are chosen as $\tau_1/\tau_2 = 1.2$, $2\pi/\omega = 3$, $A_0\omega \simeq 2.405$ [which gives $J_0(A_0\omega) = 0$], the total lattice number $2N = 80$ and the truncation number $Y = 13$.

In Figs. 2(a) and (b), we show the scaled quasi-energy E/ω versus the scaled modulation amplitude A/A_0 . In our calculation, A_0 is given by the first zero-point of $J_0(A_0\omega)$, $\tau_1/\tau_2 = 1.2$, $2\pi/\omega = 3$, and the total lattice number $2N = 80$. In the energy gap G_0 , there appear isolated zero-energy levels. In the energy gaps G_{-1} and G_1 , isolated nonzero-energy levels appear around $A/A_0 \sim 1$. In particular, isolated zero- and nonzero-energy levels can coexist in the same parametric region, see Fig. 2(b). The eigenstate profiles, which localize at two edges, indicate that these isolated levels are FESs [see Fig. 2(c)]. We know that the topological edge states in a static SSH model always appear as zero-energy modes. However, in our modulated system, there appear both zero- and nonzero-energy edge states. Naturally, there arises an open question: *Are all FESs induced by topology?*

To understand how FESs appear in the high-frequency limit, we employ the multi-scale perturbation analysis [31, 34]. By introducing a small parameter ε , we expand the solution as $u_n(z) = U_n(z_0, z_1, \dots) + \varepsilon v_n(z_{-1}, z_0, z_1, \dots) + \varepsilon^2 w_n(z_{-1}, z_0, z_1, \dots) + \varepsilon^3 \zeta_n(z_{-1}, z_0, z_1, \dots) + O(\varepsilon^4)$ with $z_{l'} = \varepsilon^{l'} z$ and $U_n = \langle u_n \rangle$, where $\langle \bullet \rangle = \varepsilon T^{-1} \int_{\varepsilon^{-1}z}^{\varepsilon^{-1}(z+T)} (\bullet)(z_{-1}) dz_{-1}$. Therefore, from Eq. (2), collecting the terms of different orders in

ε'' , one can derive the averaged coupled-mode equations

$$\begin{aligned} -i \frac{dU_{2n-1}}{dz} &= \tau_a U_{2n} + \tau_b U_{2n-2} + \delta_{(2n-1,1)} \tau_c U_2 \\ &\quad + \delta_{(2n-1,2N-1)} \tau_c U_{2N}, \\ -i \frac{dU_{2n}}{dz} &= \tau_b U_{2n+1} + \tau_a U_{2n-1} + \delta_{(2n,2)} \tau_c U_1 \\ &\quad + \delta_{(2n,2N)} \tau_c U_{2N-1}, \end{aligned} \quad (3)$$

with the Kronecker's delta-function $\delta_{(n,m)}$. Here, the effective couplings are given as $[\tau_a = \tau_1 J_0 - (\tau_1/\tau_2)\Theta, \tau_b = \tau_2 J_0 + \Theta, \tau_c = \tau_1 \Delta / (2\tau_2)]$ with $\Delta = -\omega^{-2} \tau_2^3 \sum_{m \neq 0} \sum_{j \neq \{0, -m\}} J_j J_m J_{j+m} j^{-1} m^{-1}$ and $\Theta = [1 - (\tau_1/\tau_2)^2] \Delta$. The effective couplings τ_c describe the virtual defects at boundaries, as shown in the schematic diagram in Fig. 3.

We now consider stationary solutions in the form of $U_n(z) = U_n(0)e^{iEz}$. For an infinite structure, the propagation constant E is given by $E^2 = \tau_a^2 + \tau_b^2 + 2\tau_a \tau_b \cos(k)$ with $k \in [-\pi, \pi]$. In the vicinity of $J_0(A_0\omega) = 0$, where the effective couplings (τ_a, τ_b) are weak, the edge states induced by the virtual defects have the quasi-energies $E_s^2 = \tau_a^2 + \tau_b^2 + \tau_a \tau_b [d + d^{-1}]$ with $d = \tau_c(\tau_c + 2\tau_a)/\tau_a \tau_b$ (see Supplemental Material). Obviously, when $E_s^2 > \max(E^2)$, FESs appear in the gaps G_{-1} and G_1 . Otherwise, when $E_s^2 < \min(E^2)$, FESs appear in the gap G_0 . As $\max(E^2)$ and $\min(E^2)$ correspond to $|\cos(k)| = 1$, one can obtain the cutoffs values from $E_s^2 = \max(E^2)$ and $E_s^2 = \min(E^2)$,

$$A_{cs}^{1,2}/A_0 \simeq 1 - (\tau_1 \tilde{\tau}_c \pm F_a)/(\tau_1 \tau_2), \quad (4)$$

for $\cos(k) = +1$, and

$$A_{cs}^{3,4}/A_0 \simeq 1 - (-\tau_1 \tilde{\tau}_c \pm F_b)/(\tau_1 \tau_2), \quad (5)$$

for $\cos(k) = -1$. Here, A_0 is the first root of the Bessel function $J_0(A\omega) = 0$, $F_a = \sqrt{(\tau_1 \tilde{\tau}_c)^2 + \tau_1 \tau_2 M_+}$, $F_b = \sqrt{(\tau_1 \tilde{\tau}_c)^2 + \tau_1 \tau_2 M_-}$, $\tilde{\tau}_c = \frac{\tau_1}{2\tau_2} \tilde{\Delta}$, $M_{\pm} = \frac{\tau_1}{\tau_2} \left[1 - \left(\frac{\tau_1}{\tau_2} \right)^2 \right] \tilde{\Delta} \left\{ \left[1 - \left(\frac{\tau_1}{\tau_2} \right)^2 \right] \tilde{\Delta} \mp 2\tilde{\tau}_c \right\} \pm (\tilde{\tau}_c)^2$, and $\tilde{\Delta} = \Delta|_{A \rightarrow A_0}$. These cutoff values define the boundaries between the regions with and without FESs, see the dashed blue curves in Figs. 3(a) and 3(b). Since F_b is a purely imaginary number for all $2\pi/\omega$ when $\tau_1/\tau_2 = 1.2$, in Fig. 3(a), there are no cutoff values $A_{cs}^{3,4}/A_0$. When $2\pi/\omega \rightarrow 0$, all cutoff values gradually converge into one point at $A/A_0 = 1$, and there are no FESs caused by the virtual defects.

On the other hand, as the effective model Eq. (3) is an SSH-like model, the system changes from topological to non-topological when the effective coupling are tuned from $|\tau_a| < |\tau_b|$ to $|\tau_a| > |\tau_b|$. The effective couplings (τ_a, τ_b) depend on the original couplings (τ_1, τ_2) and the driving parameters (A, ω) . We show the effective coupling strengthes $(|\tau_a|, |\tau_b|)$ versus the scaled modulation amplitude A/A_0 for $2\pi/\omega = 2$ and $\tau_1/\tau_2 = 1.2$, see the inset in Fig. 3(a). There appear two intersection points

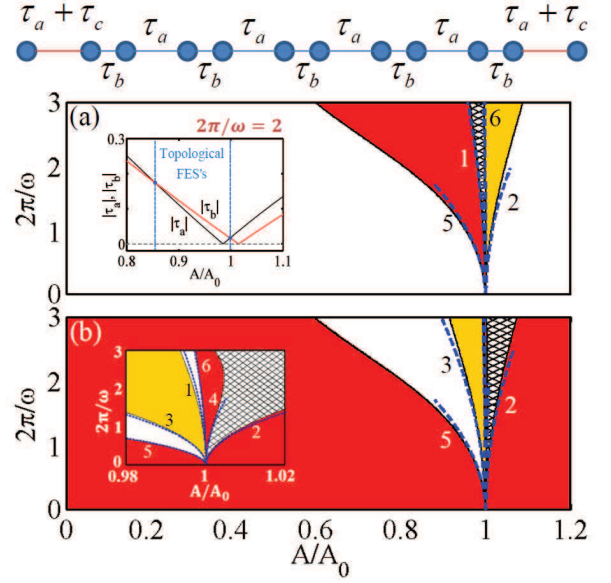


Figure 3. Phase diagram of the Floquet edge states. Top: Schematic diagram for the effective model Eq. (3). (a,b) Phase diagrams for (a) $\tau_1/\tau_2 = 1.2$ and (b) $\tau_2/\tau_1 = 1.2$. The red regions only support topological FESs, the yellow regions only support non-topological FESs, and the mesh regions support both topological and non-topological FESs. The curves 1, 2, 3 and 4 respectively correspond to the non-topological FESs cutoff values A_{cs}^1/A_0 , A_{cs}^2/A_0 , A_{cs}^3/A_0 and A_{cs}^4/A_0 . While the curves 5 and 6 respectively correspond to the topological transition points A_{ct}^5/A_0 and A_{ct}^6/A_0 , where the inset in (b) is the enlarged region nearby $A/A_0 \sim 0$. The system changes from topological to non-topological when the effective couplings are tuned from $|\tau_a| < |\tau_b|$ to $|\tau_a| > |\tau_b|$, see the inset in (a) for $2\pi/\omega = 2$.

at $|\tau_a| = |\tau_b|$ when A/A_0 increases. In the regions of $|\tau_a| < |\tau_b|$, topological FESs appear. The intersection points, where topological phase transition points occur, are given by

$$A_{ct}^{5,6}/A_0 \simeq 1 + (1 \pm \tau_1/\tau_2)^2 \tilde{\Delta}/\tau_2, \quad (6)$$

see the dashed blue curves 5 and 6 in inset of Fig. 3(b). Similarly, when $2\pi/\omega \rightarrow 0$, these two curves also gradually converge into one point at $A/A_0 = 1$. Thus, in the limit of $2\pi/\omega = 0$, the effective couplings vanish when $A/A_0 = 1$ and the modulation does not change the topological feature when A/A_0 is tuned through $A/A_0 = 1$.

To verify the above analytical results, we numerically calculate the quasi-energy spectra and the Zak phases. From the quasi-energy spectra under OBC, we indeed find several FESs appear. To distinguish topological and non-topological FESs, we then calculate Zak phases of the corresponding bulk states under PBC. We find that the Zak phase Z_{G_m} for a specific gap is either 0 or π and topological FESs only appear in a gap of nonzero Z_{G_m} .

In Fig. 3, we show the phase diagram of all possible FESs in the parameter plane $(2\pi/\omega, A/A_0)$. The

appearance of topological FESs (red regions) and non-topological FESs (yellow regions) and their coexistence (mesh regions) sensitively depend on the coupling ratio τ_1/τ_2 and the modulation parameters ($\omega, A/A_0$). In the absence of modulation, topological edge states appear only if $\tau_1/\tau_2 < 1$, otherwise no edge state appears. However, by applying a proper modulation, topological FESs may appear even if $\tau_1/\tau_2 > 1$ and also may disappear even if $\tau_1/\tau_2 < 1$. In addition to the regions of topological and non-topological FESs, there exists the region of no edge states. When $2\pi/\omega \rightarrow 0$, topological FESs appear if $\tau_1/\tau_2 < 1$ and all non-topological FESs gradually vanish at the zero-point of the Bessel function $J_0(A_0\omega) = 0$. Our numerical results clearly show all phase boundaries (the solid curves) gradually converge into one point at $A/A_0 = 1$ when $2\pi/\omega \rightarrow 0$, which well agree with our analytical results (the dashed blue curves).

Although non-topological and topological FESs can be supported by the same parameters, we find that they can not appear in the same energy gap G_0 . For a non-topological FES in the gap G_0 , its quasi-energy E_s and the bulk-state quasi-energy E should satisfy the condition $E_s^2 < \min(E^2)$. Thus, we derive a necessary but non-sufficient condition for the existence of non-topological FESs in the gap G_0 : $\tau_2 > \tau_1 > 0$ and $A \rightarrow A_0^-$. On the other hand, since the effective model (3) is an SSH-like model, the topological FESs appear if $|\tau_a|/|\tau_b| < 1$ and they always appear as zero-energy modes in the gap G_0 . However, under the conditions of $\tau_2 > \tau_1 > 0$, $A \rightarrow A_0^-$, and $|\tau_a|/|\tau_b| < 1$, there is no non-topological FES. This means that non-topological and topological FESs cannot coexist in the gap G_0 , see more details in Supplementary Material.

To explore the topological nature, we calculate the bulk topological invariant, the Zak phase [35]. For a modulated SSH system of N cells (i.e. $2N$ lattices) under PBC, by implementing a Fourier transform $c_{2n-1,\chi} = \frac{1}{\sqrt{N}} \sum_k e^{ik(2n-1)} c_{1,k,\chi}$ and $c_{2n,\chi} = \frac{1}{\sqrt{N}} \sum_k e^{ik2n} c_{2,k,\chi}$, we obtain the quasi-energy spectra and the eigenstates by diagonalizing the quasi-energy equation. The eigenstates for the l -th band, $|c_k^{(l)}\rangle = \sum_{\alpha,\chi} c_{\alpha,k,\chi}^{(l)} |\alpha, k, \chi\rangle$, are in superpositions of all Floquet-Bloch states $|\alpha, k, \chi\rangle$ with k denoting the quasi-momentum. For a gap between the $(Y+m)$ -th and $(Y+m+1)$ -th bands, its Zak phase Z_{G_m} is defined as

$$Z_{G_m} = \sum_{l=1}^{Y+m} Z^{(l)} = \sum_{l=1}^{Y+m} \left[i \oint_k \langle c_k^{(l)} | \partial_k | c_k^{(l)} \rangle dk \right]. \quad (7)$$

For a specific gap, its Zak phase Z_{G_m} is either 0 or π and the topological FESs appear only if $Z_{G_m} = \pi$ (see Supplemental Material).

In order to explore how the ratio τ_1/τ_2 affects the FESs, we show how the scaled quasi-energy spectrum depends on τ_1/τ_2 . The quasi-energy spectra and Zak

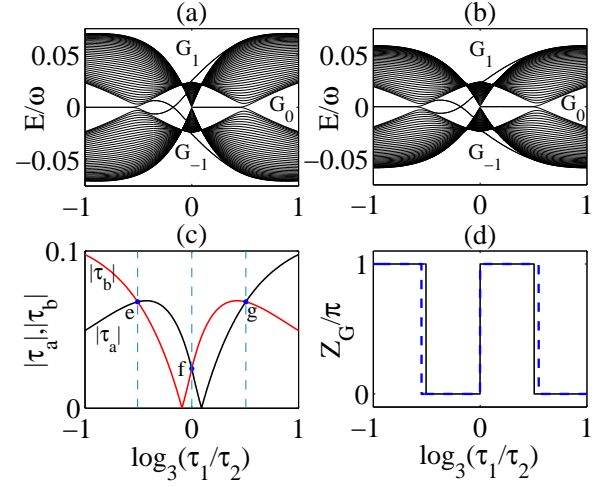


Figure 4. Scaled quasi-energy E/ω vs. coupling ratio τ_1/τ_2 . (a) Band-gap structure of the effective model (3). (b) Band-gap structure of the original model (2). (c) Effective coupling strengths ($|\tau_a|, |\tau_b|$) vs. the coupling ratio τ_1/τ_2 . (d) The Zak phases for the gap G_0 , in which the black and dashed blue lines correspond to the effective and original models, respectively. The parameters are chosen as $A/A_0 = 0.98$, $2\pi/\omega = 3$, $A_0\omega \simeq 2.405$, the total lattice $2N = 80$ and the truncation number $Y = 13$.

phases show that, even when the modulation frequency is not very high, the effective model may well explain the behaviors in the original system. The deviation between the effective and original models decreases with the modulation frequency and gradually vanishes in the high-frequency limit. In Fig. 4, we show the quasi-energy spectra, the effective couplings and Zak phases for $A/A_0 = 0.98$ and $2\pi/\omega = 3$. Although the quasi-energies have small differences, the band-gap structures are almost the same, in which both zero and nonzero FESs may appear in different gaps, see Figs. 4(a) and 4(b). From the effective model, topological FESs are always zero-energy modes and only appear in the gap G_0 when $|\tau_a|/|\tau_b| < 1$, see Figs. 4(a) and 4(c). In addition to the topological FESs, due to the modulation-induced virtual defects, there also exist non-topological FESs in different gaps. Moreover, the band-gap structures show that topological and non-topological FESs can not appear in the same gap, which confirms our previous analytical analysis. From the Zak phases, the effective and original models show similar topological phase transitions, but the transition points show small deviations dependent upon the modulation frequency, see Fig. 4(d).

In summary, we have studied the Floquet edge states in arrays of curved optical waveguides described by the periodically modulated SSH model. We have revealed that the behavior of quasi-energy spectra and Zak phases suggest that topological and non-topological edge states may be supported by the same parameters, but they always appear in different energy gaps. Without any embedded

or nonlinearity-induced defects, these edge states originate from the interplay between the bulk band topology and periodic modulations. We have derived analytically the boundaries between different topological phases, and have verified these results numerically. We believe our work provides new perspectives for topological photonics govern by periodic modulations, and it can be employed for a control of topological phase transitions. Although our analysis has been performed for arrays of periodically curved optical waveguides, it can be applicable to other lattice systems such as ultracold atoms in optical lattices [36, 37], photonic crystals [18], and discrete quantum walks [38, 39].

This work was supported by the National Natural Science Foundation of China (NNSFC) under Grants No. 11574405 and No. 11465008, and by the Australian Research Council. Both B. Zhu and H. Zhong made equal contributions.

* Corresponding author.

Email: lichaoh2@mail.sysu.edu.cn, chleecn@gmail.com.

- [1] L. Lu, J. D. Joannopoulos, and M. Soljacic, “Topological photonics,” *Nature Photonics* **8**, 821–829 (2014).
- [2] F. D. M. Haldane and S. Raghu, “Possible realization of directional optical waveguides in photonic crystals with broken time-reversal symmetry,” *Phys. Rev. Lett.* **100**, 013904–4 (2008).
- [3] S. Raghu and F. D. M. Haldane, “Analogues of quantum-Hall-effect edge states in photonic crystals,” *Phys. Rev. A* **78**, 033834–21 (2008).
- [4] Z. Wang, Y. D. Chong, J. D. Joannopoulos, and M. Soljacic, “Observation of unidirectional backscattering-immune topological electromagnetic states,” *Nature* **461**, 772–U20 (2009).
- [5] R. O. Umucalilar and I. Carusotto, “Artificial gauge field for photons in coupled cavity arrays,” *Phys. Rev. A* **84**, 043804–8 (2011).
- [6] K. J. Fang, Z. F. Yu, and S. H. Fan, “Realizing effective magnetic field for photons by controlling the phase of dynamic modulation,” *Nature Photonics* **6**, 782–787 (2012).
- [7] A. B. Khanikaev, S. H. Mousavi, W. K. Tse, M. Kargarian, A. H. MacDonald, and G. Shvets, “Photonic topological insulators,” *Nat. Mater.* **12**, 233–239 (2013).
- [8] Y. E. Kraus, Y. Lahini, Z. Ringel, M. Verbin, and O. Zeitlinger, “Topological states and adiabatic pumping in quasicrystals,” *Phys. Rev. Lett.* **109**, 106402–5 (2012).
- [9] M. C. Rechtsman, J. M. Zeuner, Y. Plotnik, Y. Lumer, D. Podolsky, F. Dreisow, S. Nolte, M. Segev, and A. Szameit, “Photonic Floquet topological insulators,” *Nature* **496**, 196–200 (2013).
- [10] M. Hafezi, S. Mittal, J. Fan, A. Migdall, and J. M. Taylor, “Imaging topological edge states in silicon photonics,” *Nature Photonics* **7**, 1001–1005 (2013).
- [11] G. Q. Liang and Y. D. Chong, “Optical resonator analog of a two-dimensional topological insulator,” *Phys. Rev. Lett.* **110**, 203904–5 (2013).
- [12] M. Pasek and Y. D. Chong, “Network models of photonic Floquet topological insulators,” *Phys. Rev. B* **89**, 075113–10 (2014).
- [13] W. C. Hu, J. C. Pillay, K. Wu, M. Pasek, P. P. Shum, and Y. D. Chong, “Measurement of a topological edge invariant in a microwave network,” *Phys. Rev. X* **5**, 011012–7 (2015).
- [14] L. H. Wu and X. Hu, “Scheme for achieving a topological photonic crystal by using dielectric material,” *Phys. Rev. Lett.* **114**, 223901–5 (2015).
- [15] C. He, X. C. Sun, X. P. Liu, M. H. Lu, Y. Chen, L. Feng, and Y. F. Chen, “Photonic topological insulator with broken time-reversal symmetry,” *Proc. Natl. Acad. Sci. U. S. A.* **113**, 4924–4928 (2016).
- [16] F. Gao, Z. Gao, X. H. Shi, Z. J. Yang, X. Lin, H. Y. Xu, J. D. Joannopoulos, M. Soljacic, H. S. Chen, L. Lu, Y. D. Chong, and B. L. Zhang, “Probing topological protection using a designer surface plasmon structure,” *Nat. Commun.* **7**, 11619–9 (2016).
- [17] Y. Lumer, Y. Plotnik, M. C. Rechtsman, and M. Segev, “Self-localized states in photonic topological insulators,” *Phys. Rev. Lett.* **111**, 243905–5 (2013).
- [18] J. M. Zeuner, M. C. Rechtsman, Y. Plotnik, Y. Lumer, S. Nolte, M. S. Rudner, M. Segev, and A. Szameit, “Observation of a topological transition in the bulk of a non-Hermitian system,” *Phys. Rev. Lett.* **115**, 040402–5 (2015).
- [19] M. S. Rudner, N. H. Lindner, E. Berg, and M. Levin, “Anomalous edge states and the bulk-edge correspondence for periodically driven two-dimensional systems,” *Phys. Rev. X* **3**, 031005–15 (2013).
- [20] A. Gomez-Leon and G. Platero, “Floquet-Bloch theory and topology in periodically driven lattices,” *Phys. Rev. Lett.* **110**, 200403–5 (2013).
- [21] A. P. Slobozhanyuk, A. N. Poddubny, A. E. Miroshnichenko, P. A. Belov, and Yu. S. Kivshar, “Subwavelength topological edge states in optically resonant dielectric structures,” *Phys. Rev. Lett.* **114**, 123901–5 (2015).
- [22] C. Poli, M. Bellec, U. Kuhl, F. Mortessagne, and H. Schomerus, “Selective enhancement of topologically induced interface states in a dielectric resonator chain,” *Nat. Commun.* **6**, 6710–5 (2015).
- [23] D. Leykam, M. C. Rechtsman, and Y. D. Chong, “Anomalous topological phases and unpaired Dirac cones in photonic Floquet topological insulators,” *Phys. Rev. Lett.* **117**, 013902–6 (2016).
- [24] Y. G. Ke, X. Z. Qin, F. Mei, H. H. Zhong, Yu. S. Kivshar, and C. Lee, “Topological phase transitions and threshold pumping of light in photonic waveguide arrays,” *Laser Photon. Rev.* **10**, 995–1001 (2016).
- [25] L. J. Maczewsky, J. M. Zeuner, S. Nolte, and A. Szameit, “Observation of photonic anomalous Floquet topological insulators,” *Nat. Commun.* **8**, 13756–7 (2017).
- [26] S. Mukherjee, A. Spracklen, M. Valiente, E. Andersson, P. Ohberg, N. Goldman, and R. R. Thomson, “Experimental observation of anomalous topological edge modes in a slowly driven photonic lattice,” *Nat. Commun.* **8**, 13918–7 (2017).
- [27] Y. Hatsugai, “Chern number and edge states in the integer quantum Hall-effect,” *Phys. Rev. Lett.* **71**, 3697–3700 (1993).
- [28] Y. Hatsugai, “Edge states in the integer quantum Hall-effect and the Riemann surface of the Bloch function,” *Phys. Rev. B* **48**, 11851–11862 (1993).
- [29] M. Hafezi, “Measuring topological invariants in photonic

- systems,” *Phys. Rev. Lett.* **112**, 210405–5 (2014).
- [30] S. Mittal, S. Ganeshan, J. Y. Fan, A. Vaezi, and M. Hafezi, “Measurement of topological invariants in a 2D photonic system,” *Nature Photonics* **10**, 180–184 (2016).
 - [31] I. L. Garanovich, A. A. Sukhorukov, and Yu. S. Kivshar, “Defect-free surface states in modulated photonic lattices,” *Phys. Rev. Lett.* **100**, 203904–4 (2008).
 - [32] A. Szameit, I. L. Garanovich, M. Heinrich, A. A. Sukhorukov, F. Dreisow, T. Pertsch, S. Nolte, A. Tunnermann, and Yu. S. Kivshar, “Observation of defect-free surface modes in optical waveguide arrays,” *Phys. Rev. Lett.* **101**, 203902–4 (2008).
 - [33] W. P. Su, J. R. Schrieffer, and A. J. Heeger, “Solitons in polyacetylene,” *Phys. Rev. Lett.* **42**, 1698–1701 (1979).
 - [34] Yu. S. Kivshar and S. K. Turitsyn, “Spatiotemporal pulse collapse on periodic potentials,” *Phys. Rev. E* **49**, R2536–R2539 (1994).
 - [35] J. Zak, “Berry’s phase for energy-bands in solids,” *Phys. Rev. Lett.* **62**, 2747–2750 (1989).
 - [36] M. Atala, M. Aidelsburger, J. T. Barreiro, D. Abanin, T. Kitagawa, E. Demler, and I. Bloch, “Direct measurement of the Zak phase in topological Bloch bands,” *Nature Physics* **9**, 795–800 (2013).
 - [37] E. J. Meier, F. A. An, and B. Gadway, “Observation of the topological soliton state in the Su-Schrieffer-Heeger model,” *Nat. Commun.* **7**, 13986–6 (2016).
 - [38] F. Cardano, A. D’Errico, A. Dauphin, M. Maffei, B. Piccirillo, C. de Lisio, G. De Filippis, V. Cataudella, E. Santamato, L. Marrucci, M. Lewenstein, and P. Massignan, “Detection of Zak phases and topological invariants in a chiral quantum walk of twisted photons,” *Nat. Commun.* **8**, 15516–7 (2017).
 - [39] E. Flurin, V. V. Ramasesh, S. Hacohe-Gourgy, L. S. Martin, N. Y. Yao, and I. Siddiqi, “Observing topological invariants using quantum walks in superconducting circuits,” *Phys. Rev. X* **7**, 031023–6 (2017).